Int. J. Multiphase Flow Vol. 17, No. 5, pp. 553–572, 1991
Printed in Great Britain.

0301-9322/91 $3.00 + 0.00

AN EXPERIMENTAL STUDY ON LOCAL INTERFACIAL PARAMETERS IN A HORIZONTAL BUBBLY TWO-PHASE FLOW

G. KOCAMUSTAFAOGULLARI and Z. WANG
Department of Mechanical Engineering, University of Wisconsin-Milwaukee, P.O. Box 784, Milwaukee, WI 53201, U.S.A.

(Received 14 January 1991; in revised form 21 April 1991)

Abstract—The internal phase distribution of cocurrent, air–water bubbly flow in a 50.3 mm dia transparent pipeline has been experimentally investigated by using a double-sensor resistivity probe. Liquid and gas volumetric superficial velocities ranged from 3.74 to 5.71 and 0.25 to 1.37 m/s, respectively, and average void fractions ranged from 4.30 to 22.5%. The local values of void fractions, interfacial area concentration, mean bubble diameter and bubble interface velocity, chord-length and frequency distributions were measured.

The experimental results indicate that the void fraction, interfacial area concentration and bubble frequency have local maxima near the upper pipe wall, and the profiles tend to flatten with increasing void fraction. The observed peak void fraction can reach 0.65, the peak interfacial area can go to 900–1000 m^2/m^3, and the bubble frequency can reach a value of 2200/s. These ranges of values have never been reported for vertical bubbly flows. It is found that either decreasing the liquid flow rate or increasing the gas flow would increase the local void fraction, the interfacial area concentration and the bubble frequency.

The axial bubble interface velocity and the Sauter mean diameter profiles show a relatively uniform distribution except near the upper pipe wall, where a sharp reduction in the velocity and mean diameter occurs. The local bubble velocity and the mean diameter generally increase with the gas flow rate.

Key Words: Bubbly two-phase flow, interfacial area concentration, local void fraction distribution, local interfacial parameters, bubble size, distribution

1. INTRODUCTION

Advances in the study of the two-phase flow increasingly require detailed internal flow structure information upon which theoretical models can be formulated. The void fraction and interfacial area are two fundamental geometrical parameters characterizing the internal structure of two-phase flow. The void fraction represents the phase distributions and is a required parameter for hydrodynamic and thermal calculations in various industrial processes. On the other hand, the interfacial area describes the available interfacial area for the interfacial transport of mass, momentum and energy in steady and transient two-phase flows and is a required parameter for two-fluid model formulation. However, little information is currently available on these parameters, and it is limited to vertical two-phase flow configurations. Particularly, there exists very little knowledge on the local interfacial area concentration in spite of its importance in multidimensional two-fluid model analysis (Bouré 1978; Ishii & Kocamustafaogullari 1982).

Several methods are available at present to measure interfacial area concentration in gas–liquid and liquid–liquid two-phase flows. These are photographic, light attenuation, ultrasonic attenuation, double-sensor probe and chemical absorption methods. Detailed reviews of these methods have been given by Veteau & Morel (1982), Veteau (1981) and Ishii & Mishima (1981). However, these methods for measuring the interfacial area concentration are effective only for certain idealized cases, e.g. only an average interfacial area can be measured by the chemical absorption method (Danckwerts 1970; Sharma & Danckwerts 1970; Schumpe & Deckwer 1980, 1982). The photographic and light attenuation methods cannot be used with opaque walls and are limited to transparent dispersed two-phase flows with volumetric concentrations of less than a few percent (Akita & Yoshida 1974; Yanz *et al.* 1986; Calderbank 1958; McLaughlin & Rushton 1973; Ohba & Itoh 1978a, b; Ohba *et al.* 1978). The ultrasonic method is not restricted to such conditions, and thus expands the measurement of the interfacial area concentration beyond the presently available range of fluids and non-opaque systems (Straus *et al.* 1986; Jones *et al.* 1986; Bensler *et al.* 1987).

However, the ultrasonic attenuation method is limited to low void fraction bubbly systems and yields a chord-averaged value of the interfacial area concentration.

In view of the intention to measure local interfacial variables in a horizontal bubbly two-phase flow with local void fractions possibly ranging from 0 to 60–65%, it is inevitable that a probe method must be used. An evaluation of potential probe methods resulted in the selection of the electrical resistivity probe because of the relatively simple instrumentation and the positive results for conducting liquids presented in the literature. In the present work, the local interfacial parameters in a horizontal bubbly two-phase flow have been studied experimentally by using the double-sensor electrical resistivity probe method. Local void fractions, interfacial area concentration, interfacial velocity, local bubble chord-length, size and frequency distributions have been measured, and the results are documented here. Furthermore, the dependence of the local parameters on other flow variables are also presented.

2. DOUBLE-SENSOR RESISTIVITY PROBE METHOD

2.1. Measurement principle

The electrical resistivity probe method was first proposed by Neal & Bankoff (1963) for the determination of bubble size and velocity in vertical bubbly flows. Since then the double-sensor resistivity probe has been used by Park *et al.* (1969) and Rigby *et al.* (1970) for the determination of bubble parameters in three-phase fluidized beds, by Hoffer & Resnick (1975) for steady- and unsteady-state measurements in liquid–liquid dispersions, by Burgess & Calderbank (1975) for measurements of bubble parameters in single-bubbly flow, by Serizawa *et al.* (1975), Herringe & Davis (1976) and Liu (1989) for the study of structural parameters as well as of the structural development of gas–liquid bubbly flows, and by Veteau (1981) for the measurement of local interfacial area concentrations.

In principle, the electrical resistivity probe method consists of the instantaneous measurement of local electrical resistivity in the two-phase mixture by means of a sensor electrode. In an air–water flow the air can be considered as electrically insulating, whereas water is electrically conducting. When the sensor is in contact with the liquid, the circuit is closed. On the other hand, when it is in contact with a bubble, the circuit will open. Since the circuit is open or closed depending on whether the sensor is in contact with gas or liquid, the voltage drop across a sensor fluctuates between a V_{min} and a V_{max}. In the case of a double-sensor probe method, each sensor and the return electrodes are connected to their own measuring circuits and, therefore, each sensor is used independently as a phase identifying device. Furthermore, from the timing of the shift in the voltage between V_{min} and V_{max}, the time when the gas–liquid interface passes the sensor can be recorded. Therefore, two pieces of parallel and independent information related to the phase identification and the transit time of the gas–liquid interface are obtained. A schematic diagram indicating a typical time history record of signals from a double-sensored electrical resistivity probe in bubbly flow is illustrated in figure 1(a, b).

As seen from the figure, the signals deviate from the ideal two-state square-wave signals. This deviation is largely due to the finite size of the sensor causing flow disruption and the possible deformation of the interface before the sensor enters from one phase to the other. The trailing edges are generally steeper than the leading edges. This difference is probably due to the wetting of the sensor by the residual liquid when the sensor is in the gas phase. A proper threshold voltage has to be used as a phase identification criterion. The value of the threshold voltage is determined by processing the data for void fraction and comparing it with the average void fraction measured by the quick-closing valve technique.

2.2. Double-sensor resistivity probe design and signal processing

A typical double-sensor resistivity probe is shown in figure 2. It consists of two identical stainless-steel wire sensors of 0.25 mm dia. Their tips are 2.5 mm apart. They are completely insulated from the environment except at their tips. The tips are sharpened to a fine needle point to minimize deformation of bubbles on impact with the sensors. The two sensors are placed next to each other but insulated from each other. The body which holds the sensor acts as the return

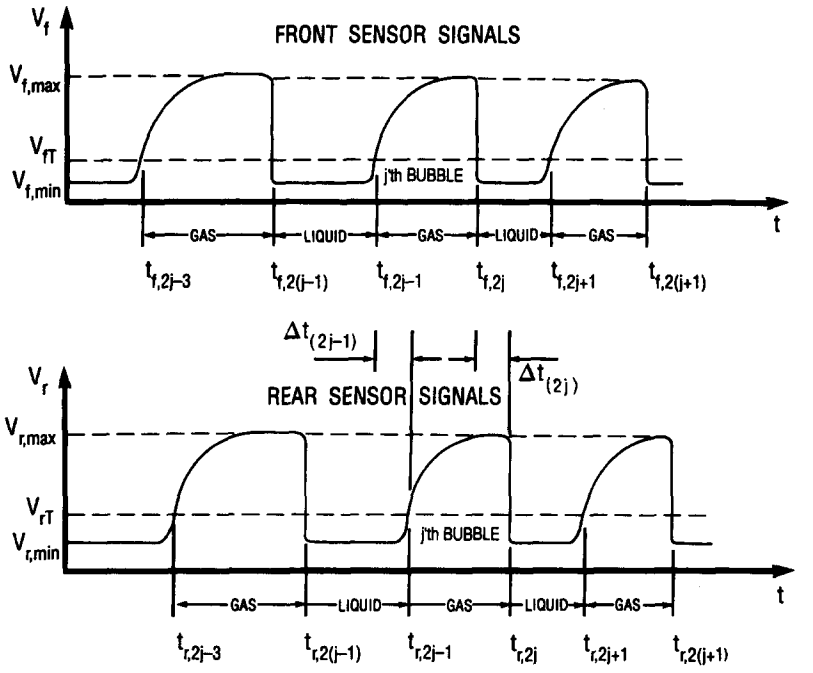

Figure 1. Schematic of the output signals: (a) front sensor; (b) rear sensor.

electrode. These two sensors are welded onto gold-plated wires of 0.8 mm dia. The complete assembly fits into a probe holder from which coaxial wires run to the electronic circuit. The electronic circuit uses a 4.5 V d.c. power supply. Variable resistors are used to enable adjustment of the maximum and minimum voltage signals.

It was found that the proper distance, L, between two sensors was critical for analyzing the experimental data. Preliminary experiments were conducted to determine a proper distance between two probe tips. The distance was dictated by possible bubble size and bubble velocity. It was

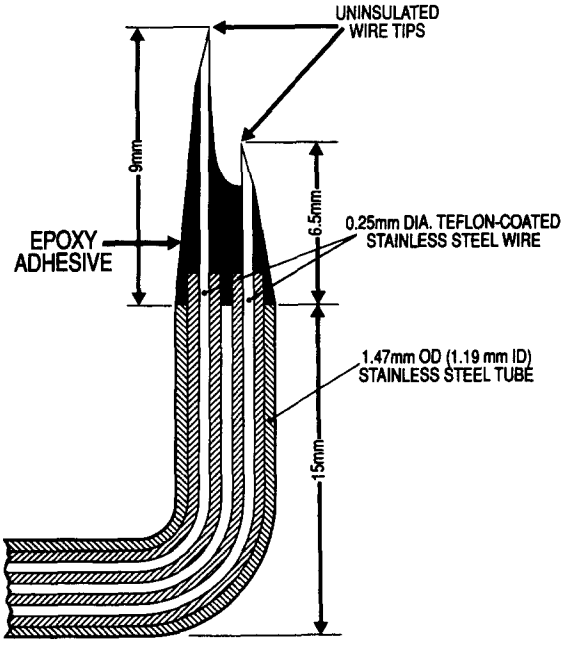

Figure 2. Double-sensor electrical resistivity probe design.

decided that 2.5 mm was the appropriate separation distance for the horizontal flow. It is to be noted that a very small distance results in inaccuracies in time duration measurements, since it requires very high sampling frequencies or very small bubble velocities. During the present experiments a sampling rate of 20 kHz was used. On the other hand, if the distance is too large, then there is a strong possibility of misinterpretation of signals since multibubble contact may occur between two signals originating from the same bubble. Even though most investigators in the past have used a distance of 5 mm in their vertical bubbly flow experiments, it was found that 5 mm was too large for the horizontal two-phase flow experiments, since maximum packing of bubbles almost always occurs toward the top of the pipe, which requires a smaller separation distance.

As illustrated in figure 1(a, b), the experimental data was obtained in the form of a voltage signal as a function of time from the front and rear sensors of a probe. The correct interpretation of data involves the identification of gas and liquid phases. The first step is to set a threshold voltage at which the signal representing the beginning of the gas phase for an isolated bubble can be identified. However, it was observed that the threshold voltage level may drift during the experiments due to the probe contamination. This difficulty was overcome by dividing the data into several blocks within the total sampling time domain. As an isolated bubble contacts the previously wetted probe, output signals increase from the value of a near V_{min} to a near V_{max}, and decrease abruptly to the value of V_{min} as the bubble moves away. Identification of such a bubble is straightforward. However, for closely compacted bubbles that are observed in a horizontal bubbly flow, the time duration of the liquid phase contacting a probe sensor is very short. Hence, before the sensor tip becomes totally wet, it could be in contact with another bubble. In this case the voltage signal varies between a local minimum above the threshold voltage and the gas level. To identify such a bubble the threshold voltage and the slope of the signal was used in combination for distinguishing phases. A linear programming method was developed to reach a desired convergence.

After distinguishing the phases, the next step is the identification of signals originating from the same bubble. In this case, the right selection of two closely corresponding signals from each sensor is important, since the two signals detected by the front and rear sensors do not always corespond to the same bubble, and the residence time intervals of the gas and or liquid phases at the sensors are not exactly the same. The signal validation was made by judging whether the following series of conditions are satisfied:

1. For a forward motion of the bubbles, the front sensor signal rises or falls before the rear sensor does. Therefore, referring to figure 1, the following condition should be satisfied:

$$t_{f(2j-1)} < t_{f(2j)} \quad \text{and} \quad t_{r(2j-1)} < t_{r(2j)}, \quad j = 1, \ldots, N, \tag{1}$$

   where f and r, respectively, denote the front and rear sensors; $t_{(2j-1)}$ is the time the front and rear sensor tips enter into the bubble and t_{2j} is the time the sensor tips enter into the liquid phase. N is the number of bubbles passing through a given sensor in the total sampling time T.
2. The residence time of a bubble, i.e. the width of the signals, the amplitude and the height above the threshold voltage of the signals for the front and rear sensors should be comparable to ensure that both sensors detect the same bubble. Hence, the following conditions should be also satisfied:

$$(t_{f(2j)} - t_{f(2j-1)}) \simeq (t_{r(2j)} - t_{r(2j-1)}), \quad j = 1, \ldots, N,$$

$$V_f(t_{f(2j)}) - V_f(t_{f(2j-1)}) \simeq V_r(t_{r(2j)}) - V_r(t_{r(2j-1)}), \quad j = 1, \ldots, N,$$

   and

$$V_f(t_{f(2j-1)}) - V_{fT} \simeq V_r(t_{r(2j-1)}) - V_{rT}, \quad j = 1, \ldots, N. \tag{2}$$

3. The time difference between the front and rear sensor should be limited by the following condition:

$$\Delta t_{min} \leqslant t_{r(2j)} - t_{f(2j)} \leqslant \Delta t_{max}$$

$$\Delta t_{min} \leqslant t_{r(2j-1)} - t_{f(2j-1)} \leqslant \Delta t_{max}, \tag{3}$$

where Δt_{min} and Δt_{max} are the time limits corresponding to the maximum and minimum bubble velocities, respectively. Therefore, Δt_{min} and Δt_{max} should be determined by the combination of the distance between two sensor tips, L, and the flow conditions such as superficial velocities. In our experiments L is fixed to be 2.5 mm, and the flow conditions are limited by $0.25 \leqslant \langle j_G \rangle \leqslant 1.59$ m/s. In view of this physical reasoning, Δt_{min} is equated to the smallest data acquisition time interval, i.e. 5×10^{-5} s, whereas Δt_{max} is taken as 40 time intervals, which becomes 2×10^{-3} s for a sampling frequency of 20 kHz. For our experimental conditions and probe distance, these values are believed to be appropriate to cover a relatively wide range of possible bubble velocities.

2.3. *Local void fraction*

The local void fraction (ϵ) at any location r can be obtained by either front or rear probe sensor tips. It is defined as a time average of the concentration $\delta(r, t)$ by

$$\epsilon(r) = \lim_{T \to \infty} \int_0^T \delta(r, t)\, dt, \qquad [4]$$

where δ, as a function of space coordinates r and time t, $= 1$ if the probe tip is in gas and $\delta = 0$ if the tip is in the liquid phase. As the signal is given in discrete form, [4] can be written from figure 1 either for the front or rear probe as follows:

$$\epsilon(r) = \frac{1}{T} \sum_{j=1}^{N} (t_{2j} - t_{2j-1}). \qquad [5]$$

2.4. *Local bubble interface velocity and velocity spectrum*

The local bubble interface velocity is determined from the signals of two probes. A bubble which contacts the first probe will, in general, subsequently make contact with the second probe. The time delay between the two contact signals is a measure of the bubble velocity. The bubble interface velocity component in the axial direction can be expressed as

$$u_b = \frac{L}{\Delta t}, \qquad [6]$$

where Δt is the time delay and L is the distance between two sensor tips.

The multichannel method and cross-correlation techniques are used in the determination of the time delay. In the multichannel method, the bubble transport time signals are processed through a computer program to identify signals from the same bubble. This process thus eliminates miscounting of bubbles. The interface velocity for a specified bubble is then given by

$$u_{bj} = \frac{L}{\Delta t_{(2j-1)}}, \quad j = 1, 2, \ldots, N, \qquad [7]$$

where the index j refers to a jth bubble. Then using the multichannel method, the bubble velocity signals are proportionally transferred into equally spaced channels. The local bubble velocity component in the flow direction, $u_b(r)$, and the standard deviation of the bubble velocity spectrum, $s(r)$, are given by

$$u_b(r) = \frac{\sum_{k=1}^{N_k} n_k u_{nk}(r)}{\sum_{k=1}^{N_k} n_k} \qquad [8]$$

and

$$S(r) = \left\{ \frac{\sum_{k=1}^{N_k} n_k [u_{bk}(r) - u_b(r)]^2}{\sum_{k=1}^{N_k} n_k} \right\}^{1/2}, \qquad [9]$$

where u_{bk} is the instantaneously measured local axial bubble velocity in the kth channel, n_k is the total count for the kth channel and N_k is the number of channels.

The cross-correlation function, which gives the most probable time delay, is also computed. If $u_f(t)$ and $u_r(t)$ are two signals from the front and the rear sensors, respectively, then the cross-correlation function $F_{u_f u_r}(\Delta t_m)$ is given by

$$F_{u_f u_r}(\Delta t_m) = \frac{1}{T}\int_0^T u_f(t - \Delta t_m) u_r(t)\, dt. \quad [10]$$

The maximum value of $F_{u_f u_r}(\Delta t_m)$ yields the most probable time delay Δt_m, from which the bubble velocity is determined through the use of [6].

2.5. Local interfacial area concentration

The local interfacial area concentration at any spatial location r is given by Ishii (1977) as

$$a_i(r) = \frac{1}{T}\sum_{j=1}^{N_i} \frac{1}{|\mathbf{v}_i \cdot \mathbf{n}_i|_j}, \quad [11]$$

where T, $\mathbf{v}_i$ and $\mathbf{n}_i$ are the sampling time, interfacial velocity and unit normal vector of the interface. N_i is the total number of interfaces passing through the point within the sampling time T. Physically this local interfacial area concentration represents the probability of the interface occurring at that point.

The form of [11] indicates a possible measurement technique for determining the local interfacial area concentration. Basically it requires the measurement of the interfacial velocity and the surface direction at the point. A simplified double-sensor resistivity probe suggested by Herringe & Davis (1976), Veteau (1981) and Veteau & Charlot (1981) assumes a unidirectional flow of spherical particles. However, considering the velocity fluctuations due to turbulences or fluid particle motions, Kataoka *et al.* (1985) suggested an improved statistical model. In this model it was assumed that the direction of the interface velocity fluctuates within a maximum angle of θ_0 from the axial direction with equal probability. Then this angle θ_0 was related to the root-mean-square (r.m.s.) of fluctuating components of the velocity which can be measured by the same double-sensor probe simultaneously with the measurement of the sensor passing velocity u_{bj}. Then the local interfacial area concentrations are given by

$$\begin{aligned} a_i(r) &= \left[\frac{2}{T}\sum_{j=1}^{N} \frac{1}{|u_{bj}(r)|}\right] C(\alpha_0) \\ &= \frac{2}{LT}\sum_{j=1}^{N} [\Delta t_{(2j-1)} + \Delta t_{(2j)}] C(\alpha_0), \end{aligned} \quad [12]$$

where

$$C(\alpha_0) = \left\{1 - \cot\left(\frac{\alpha_0}{2}\right)\ln\left[\cos\left(\frac{\alpha_0}{2}\right)\right] - \tan\left(\frac{\alpha_0}{2}\right)\ln\left[\sin\left(\frac{\alpha_0}{2}\right)\right]\right\}^{-1}. \quad [13]$$

The angle α_0 is given approximately by

$$\frac{\sin 2\alpha_0}{2\alpha_0} \simeq \frac{\dfrac{1 - S^2}{u_b^2}}{\dfrac{1 + 3S^2}{u_b^2}}, \quad [14]$$

where S is the r.m.s. of the fluctuating component of the sensor passing velocity, which is conveniently expressed by [9].

Knowing the value of α_0, the time-averaged local interfacial area concentration can be calculated from the measured values of $u_b(r)$ at any location r. The measured value of $u_b(r)$ is given by [8], whereas the value of α_0 can be estimated from measured values of the statistical parameters of interfacial velocity, as given by [14]. It is to be noted that the r.m.s. of fluctuations of the axial component of interfacial velocity are assumed to be the r.m.s. of two other velocity component fluctuations, i.e. unidirectional assumption. Studies carried out by Hilgert & Hofmann (1986) on

bubble columns in a vertical pipe using an ultrasonic Doppler technique have shown that the magnitude of the axial component r.m.s. bubble velocity fluctuation is nearly equal to the radial component of the r.m.s. of the fluctuation of bubble velocity. In the present study, [12] was used to determine the local interfacial area concentration for the horizontal bubbly flow experiments.

3. EXPERIMENTAL SETUP AND PROCEDURE

3.1. Description of the flow loop

A horizontal flow loop was designed and built for the purpose of investigating the interfacial structure of horizontal two-phase flow. The overall loop schematic is illustrated in figure 3. The loop basically consists of various flanged lengths of 50.3 mm i.d. circular Pyrex glass tubings with pressure tabs installed between them. However, smaller or larger diameter test sections can be easily fitted to the loop. The entire test section is about 15.4 m in length, and it is all transparent, so that flow visualization, high-speed photography and high-speed cinematography are possible. It is designed such that various local instrumentations for two-phase flow measurements and different mixing chambers can be easily accommodated.

The air and water are used as coupling fluids. The air to the test section is supplied from the University of Wisconsin–Milwaukee central air system. It is, however, regulated through a 0.95 m^3-capacity high-pressure storage tank, and metered by a series of turbine flow meters. The water is recirculated. It is pumped from a 1.9 m^3-capacity storage tank by a stainless-steel centrifugal pump and regulated from 0 to 100% of the pump capacity by a transistor inverter. The water flow rate is measured by a series of paddlewheel flow meters assembled in a parallel configuration. As shown in figure 4 the air enters the mixing chamber from a 90° vertical leg and is injected into the water flow through a cylindrical porous media of 100 μm porosity to achieve a uniform mixing and the quick development of a bubbly two-phase flow pattern. The two-phase mixture from the test section is directed to an air–water separator. The air is vented to the atmosphere, and the water is returned to the water storage tank.

The last 1.5 m of the test section incorporates two quick-closing valves which are used for average void fraction measurements. These valves, which are pneumatically operated and electronically controlled, have a very rapid response time (in the order of milliseconds) and are synchronized through a common electrical switch to ensure simultaneous operation. The distance between the valves is long enough to minimize any experimental error. The system is protected against pressure surges.

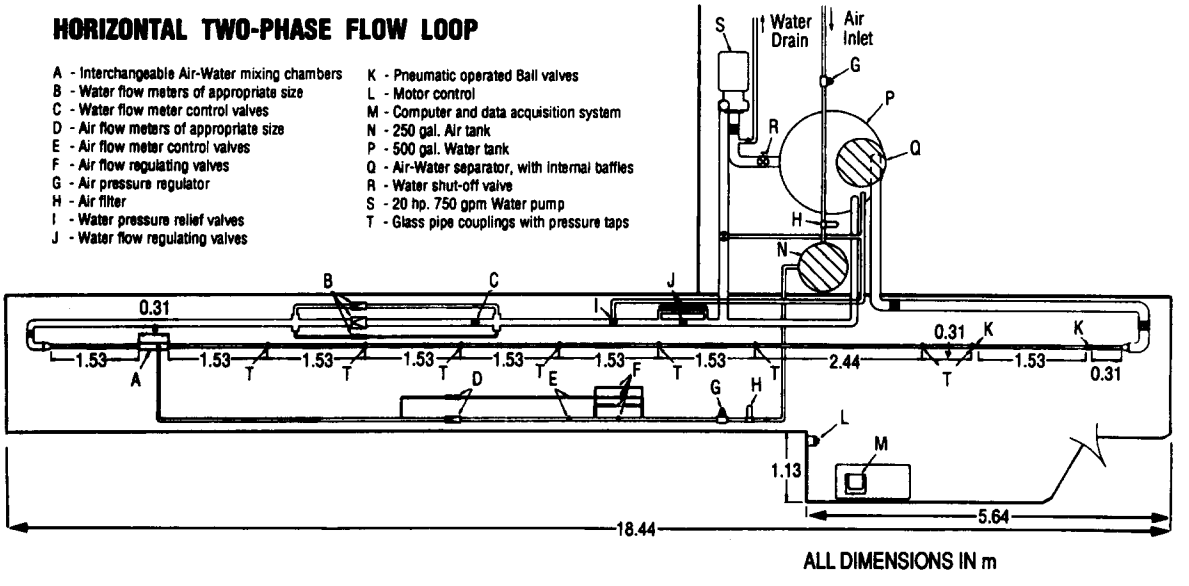

Figure 3. Schematic of the experimental flow loop.

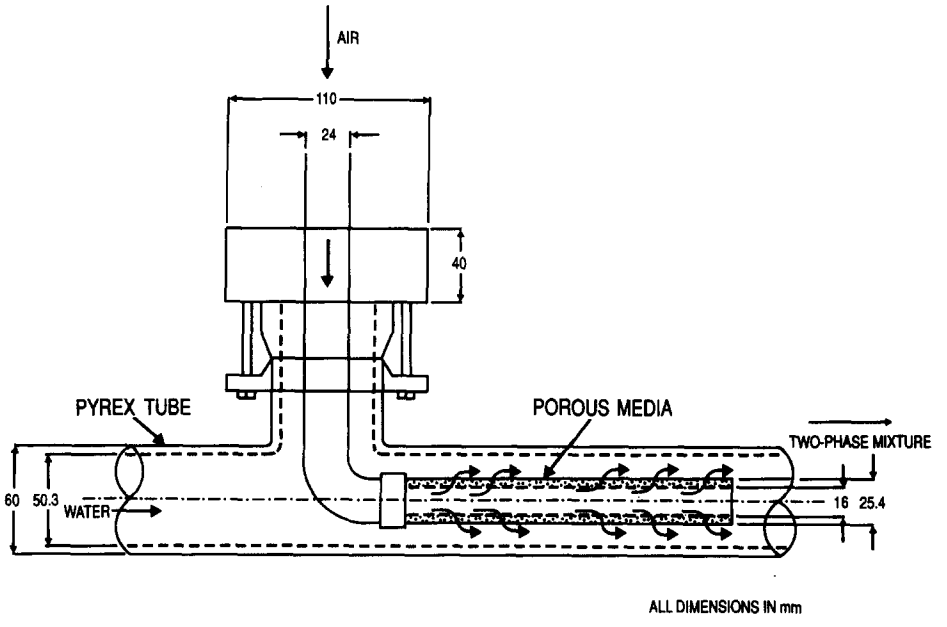

Figure 4. Schematic of the air–water mixing chamber.

Pressure transducers of the diaphragm type are utilized for both absolute pressure and differential pressure measurements. The test-section differential pressure is measured at six intervals with high-frequency transducers located 1.55 m apart. The absolute pressure transducers are located at two locations in the test section, 6.70 and 8.22 m downstream of the mixing chamber, respectively.

3.2. Experimental procedure

The experiments were carried out under fully developed bubbly flow conditions by variations in the liquid flow rate, gas flow rate and the radial position of the probe. The superficial liquid velocities ranged from 3.74 to 5.71 m/s, and the superficial gas velocities covered a range from 0.25 to 1.37 m/s. Details of the experimental conditions are summarized in table 1. At each fixed liquid superficial velocity, the gas superficial velocity was increased as long as the flow pattern was bubbly. Evidence of slug flow was indicated in the output signals and discarded from evaluation. Liquid superficial velocities higher than indicated above could not be reached due to pressure limitations of the Pyrex glass test loop. During the operation of the quick-closing valves, the pressure reached sizable proportions of the loop pressure limitations. The temperature of the water was maintained at room temperature by adding tap water to the storage tank.

The mounting and traversing mechanism for the resistivity probe is shown in figure 5. The probe was inserted through a probe support located at the bottom of a rectangular Plexiglas test section. The test section was 15 cm in length, 15 cm in height and 7.5 cm in width. A Vernier, with graduations to an accuracy of 0.0254 mm, was used to traverse the probe in a direction perpendicular to the axis of the tube; 23 locations were selected through the pipe diameter of 50.3 mm. The increments were smaller as the probe traversed toward the wall at the upper half of the tube.

For each preset experimental condition the data, including 23 probe locations, pressure drops at 6 intervals and the absolute system pressure at 2 locations, were recorded. At the end of each experimental run the quick-closing valves were operated to measure average void fraction. Experiments were interfaced with a data acquisition system utilizing a Zenith PC/AT computer with a Metrabyte DASH-16F 16-channel multifunction high-speed analog/digital I/O expansion board, and Labtech Notebook software.

Due to the large volume of data generated, the sampling rate was kept at 20 kHz for each sensor, and the sampling time was 1 s. It was found that this combination provided a sufficiently large

Table 1. Experimental conditions and comparisons of velocities

No.	$\langle j_f \rangle$ (m/s)	$\langle \epsilon \rangle$ (%)	$\bar{u}_b$ (m/s)	$\bar{u}_G$ (m/s)	$\Delta\bar{u}_b$ (%)	$\langle j_b \rangle$ (m/s)	$\langle j_G \rangle$ (m/s)	$\Delta\langle j_b \rangle$ (%)
1	3.74	5.70	4.01	4.39	−8.9	0.23	0.25	−8.8
2	3.74	10.50	4.49	4.86	−7.6	0.471	0.51	−7.6
3	3.83	15.18	4.50	4.71	−4.4	0.68	0.72	−5.6
4	3.74	18.30	5.10	5.63	−0.4	0.93	1.03	−9.7
5	4.05	6.48	4.25	4.06	−4.7	0.27	0.26	3.8
6	4.05	10.70	4.69	4.77	−1.7	0.50	0.51	−1.9
7	4.05	15.40	5.02	4.94	−1.6	0.77	0.76	−1.3
8	4.06	18.70	5.53	5.56	−0.5	1.03	1.04	−0.9
9	4.05	21.00	5.89	6.38	−7.7	1.23	1.34	−8.2
10	4.45	4.70	4.64	5.15	−9.9	0.22	0.24	−9.9
11	4.36	10.30	4.89	4.95	−1.2	0.50	0.51	−1.6
12	4.36	14.10	5.41	5.53	−2.1	0.76	0.78	−2.5
13	4.36	21.50	6.32	6.09	3.7	1.36	1.31	3.8
14	4.36	22.50	6.37	7.07	−9.9	1.43	1.59	−10.1
15	4.78	4.30	5.21	5.88	−11.4	0.22	0.25	−10.4
16	4.67	8.70	5.39	6.09	−11.5	0.47	0.53	−11.3
17	4.70	14.30	5.77	5.52	4.5	0.82	0.79	3.8
18	4.77	18.25	6.17	6.52	−5.4	1.12	1.19	−5.6
19	5.10	4.34	5.49	5.61	−2.1	0.24	0.24	0.0
20	5.10	8.02	5.60	6.05	−7.9	0.44	0.48	−6.4
21	4.98	13.90	6.32	5.76	9.7	0.88	0.80	10.0
22	4.98	20.40	6.26	6.57	−4.7	1.27	1.34	−5.2
23	5.29	12.50	6.78	6.40	5.9	0.849	0.80	−6.1
24	5.29	20.80	7.30	6.49	12.4	1.516	1.35	12.3
25	5.71	10.60	7.03	6.75	4.1	0.75	0.71	4.9
26	5.60	21.80	6.04	6.43	−6.0	1.31	1.37	−5.3

volume of data for any statistical analysis. It is to be noted that the total sampling time may seem very short when compared to earlier investigations carried out on vertical bubbly two-phase flows. However, it is also to be noted that in a horizontal bubbly two-phase flow the velocities are very high and thus it becomes essential to have a sampling rate as high as possible to record all the bubbles. This simultaneously leads to a shorter sampling time due to overall limitations on the data acquisition system.

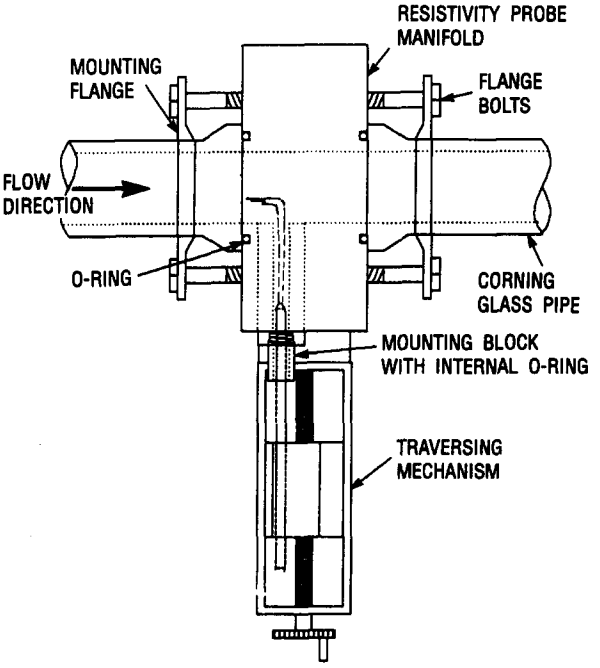

Figure 5. Mounting and traversing mechanism.

4. EXPERIMENTAL RESULTS AND DISCUSSION

4.1. Local void fraction distribution

The local void fractions were obtained independently with both front and rear sensors of the probe using the average void fraction as a convergence criterion to decide the threshold voltage. Then [5] was used to calculate the local void fractions. A sample of local void fraction distributions obtained from both sensors is shown in figure 6, and figures 7a, 7b, 8a and 8b illustrate local void fraction profiles for several flow parameter values of $\langle j_f \rangle$ and $\langle j_G \rangle$. In figures 7a, 7b, 8a and 8b only the front sensor measurements are used. The following observations can be made from these figures:

(a) The void fraction distributions obtained by front and rear probes are surprisingly close to each other, indicating the consistency in the signal processing methodology. Although signal validation was made to identify the interfaces by a series of conditions expressed by [1]–[3], it might still be possible that some bubbles contact only the front sensor and escape from the rear sensor. As a result, the front sensor tends to give a slightly higher void fraction than the rear sensor, as barely observed in figure 6.

(b) It is evident from these figures that the bubbles tend to migrate toward the upper wall under the dominating influence of buoyancy force. Thus, the void fraction under all test conditions generally showed a distinct peak near the top wall at

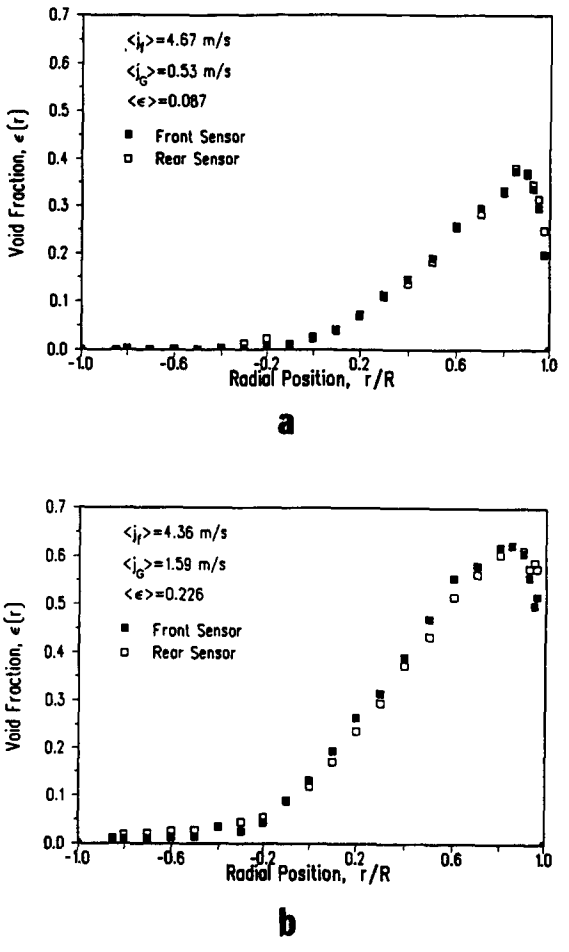

Figure 6. Local void fraction distributions obtained from the front and rear sensors.

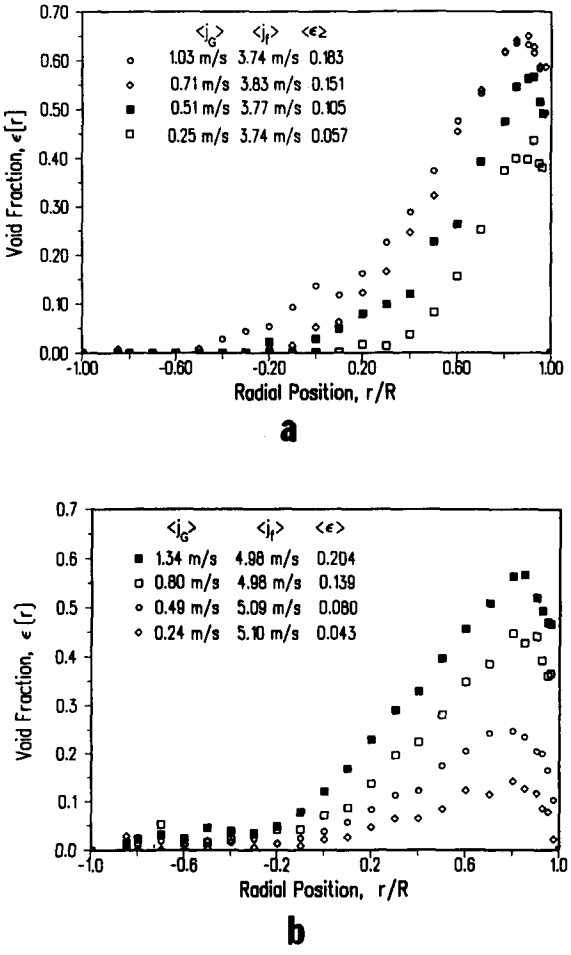

Figure 7(a). Influence of gas flow on the local void fraction distribution at low liquid flow. (b) Influence of gas flow on the local void fraction distribution at high liquid flow.

about $r/R \simeq 0.8$ to 0.9. This range corresponds to that at a 2.5–5 mm distance from the wall. When these values are compared with the observed Sauter mean bubble diameter of 2–5 mm, as documented in section 4.1, the geometry seems to explain the steep decrease in the void fraction. Besides the geometric effects, the possibility of probe interference toward the wall and the increased hydraulic resistance of the liquid path between the bubble and wall may also contribute to the sharp decline in the void fraction. This phenomenon is identical to the one that has been observed in vertical bubbly two-phase flows by Veteau (1981), Serizawa *et al.* (1975), Wang (1985) and Wang *et al.* (1987).

(c) Although the void fraction distributions tend to flatten as the average void fraction increases, the distinct peak always occurs in relatively the same location. The fact that the peak void fraction in all cases never exceeds 0.60–0.65 indicates that a maximum packing exists in the channel. Above the maximum packing limit, coalescence of bubbles occurs resulting in larger slug bubbles.

(d) The effect of increasing the gas flow rate is to increase the average void fraction and to flatten the void fraction distribution toward the bottom channel wall. Again, there was no noticeable change at the peaking positions.

(e) The effect of increasing the liquid flow rate is to decrease the average void fraction. However, there were no noticeable differences in the peaking positions, but there was a significant decrease in the value of the maximum void fraction.

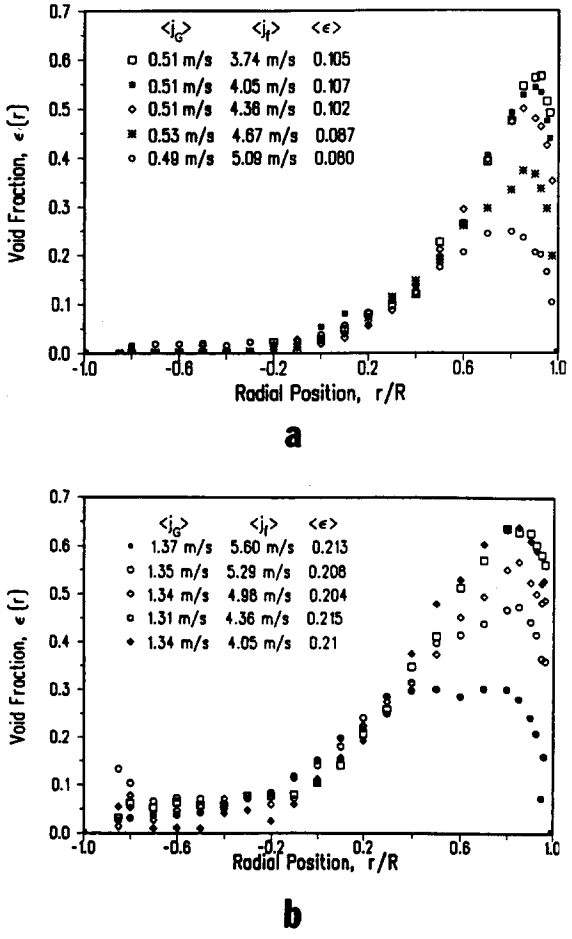

Figure 8(a). Influence of liquid flow on the local void fraction distribution at low gas flow. (b) Influence of liquid flow on the local void fraction distribution at high gas flow.

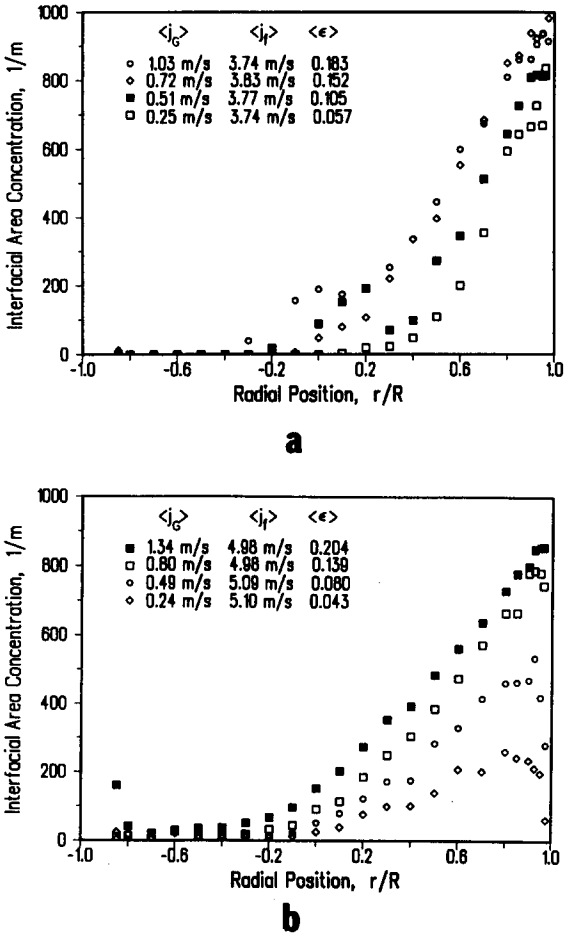

Figure 9(a). Effect of gas flow on the local interfacial area concentration profile at low liquid flow. (b) Effect of gas flow on the local interfacial area concentration profile at high gas flow.

4.2. Local interfacial area and bubble size distributions

Figures 9a, 9b, 10a and 10b show the local interfacial area concentration profiles based on [12]. It is interesting to note that the interfacial area concentration distributions have similar characteristics to those of the void fraction distributions. The interfacial area reaches a maximum at about the same location as the void fraction peak. Increasing the gas flow or decreasing the liquid flow would increase the local and overall interfacial area concentration and tend to flatten the interfacial area concentration profile.

It is important to note that the local interfacial area concentration in horizontal bubbly two-phase flow may become as high as 1000 m^2/m^3 toward the top of the channel. This range of the interfacial area concentration has never been reported for vertical bubbly flow. The higher values suggest that in this type of bubbly flow the interfacial transport of mass, momentum and heat transfer is much higher near the top portion of the tube wall.

The interfacial area concentration is strongly affected by bubble sizes, since the surface-to-volume ratio of a small bubble is larger than that of a larger bubble. Furthermore, when the bubbles are not spherical, the volume-to-surface area ratios depend on the shape of the bubble at the same void fraction.

The profiles of the interfacial area concentration and the void fraction can be used to determine the Sauter mean bubble diameter variations along the cross section. The definition of the Sauter mean bubble diameter assumes spherical bubbles and is given by

$$D_{sm} = \frac{\sum_{k=1}^{N_k} n_k D_k^3}{\sum_{k=1}^{N_k} n_k D_k^2}, \qquad [15]$$

where n_k is the number of bubbles of size D_k and N_k is the total bubble size classes.

On the other hand, the void fraction and the interfacial area concentration can be expressed, respectively, as

$$\epsilon(r) = \frac{\sum_{k=1}^{N_k} n_k V_k}{V_T} = \left(\frac{\pi}{6}\right) \frac{\sum_{k=1}^{N_k} n_k D_k^3}{V_T} \qquad [16]$$

and

$$a_i(r) = \frac{\sum_{k=1}^{N_k} n_k A_k}{V_T} = \pi \frac{\sum_{k=1}^{N_k} n_k D_k^2}{V_T}, \qquad [17]$$

where V_k is the volume of a typical bubble of size D_k in a given class k, A_k is the surface area of a typical bubble in the same class size and V_T is the total mixture volume.

From [15]–[17] it can be shown that

$$D_{sm}(r) = \frac{6\epsilon(r)}{a_i(r)} \qquad [18]$$

Based on [18], typical Sauter mean diameter distributions are illustrated in figure 11(a, b) at various gas as well as various liquid fluxes. From this figure it may be observed that the Sauter mean diameters are in the range of 2–5 mm, depending on the location and flow conditions. The profiles show relatively small variations over most of the flow channel cross section except near the wall region. The bubble size tends to reduce close to the wall region. Generally there is no double size peaking found, as reported for vertical bubbly flow by Michiyoshi & Serizawa (1986), Matsui (1984) and Liu (1989). The bubble diameter generally shows an increase with the gas flow rate, although the influence is not significant. By comparing two figures it may be observed that increasing liquid flow rate results in a more homogeneous distribution of the bubbles.

Figure 12 illustrates the variation in the average interfacial area concentration as a function of the averaged void fraction. Figure 12 is not intended to be a correlation between $\langle a_i \rangle$ and $\langle \epsilon \rangle$. It is obvious from [18] that besides the void fraction, the bubble size also has a very important effect

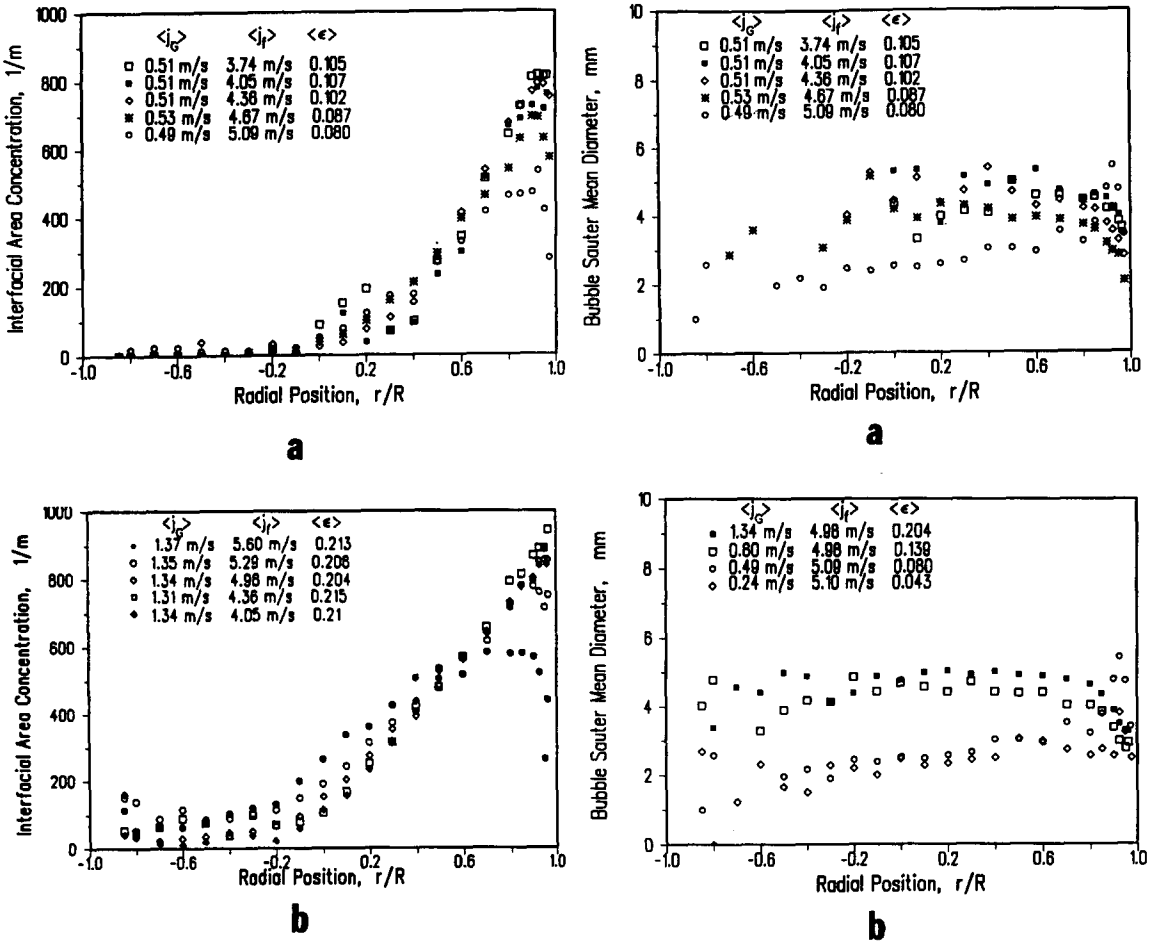

Figure 10(a). Effect of liquid flow on the local interfacial area concentration profile at low gas flow. (b) Effect of liquid flow on the local interfacial area concentration at high gas flow.

Figure 11. Sauter mean diameter profiles: (a) effect of liquid flow; (b) effect of gas flow.

in determining the interfacial area concentration. However, considering small variations in the mean diameter, the behavior observed in figure 12 is not surprising.

4.3. Local bubble interface velocity

The local bubble interface velocity in the axial direction was determined from the signals of two resistivity probe tips using [6] and [8]. Samples of the mean local bubble velocity distributions

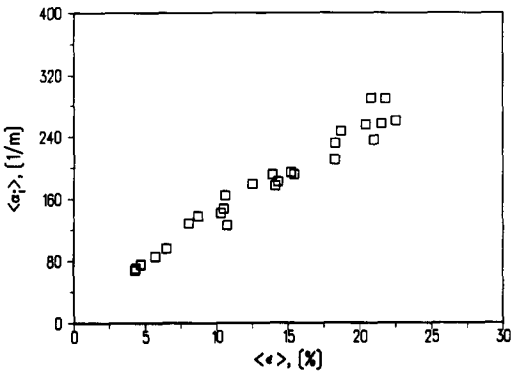

Figure 12. Average interfacial area concentration as a function of void fraction.

calculated from the bubble velocity spectrum and also from the cross-correlation method are shown in figure 13(a, b). The bubble velocity spectrum at every local position covered a range of bubble velocities approximately following a Poisson distribution. A typical velocity spectrum is also illustrated in figure 14(a, b). The following observations can be made from these figures.

There was no evidence to suggest a proportionate correspondence between local void fraction and bubble velocity distributions, as suggested by Van der Welle (1985) and Beattie (1972) for vertical flow. There were no peaks in bubble velocity profiles corresponding to those observed toward the top wall peaking void and interfacial area concentration profiles. On the contrary, the velocity profiles show a fairly uniform distribution over a large portion of the flow area, except for the wall region.

It can be observed that an increase in either the liquid flow rate or gas flow rate increases the bubble velocity. The mean bubble velocity near the upper wall decreases, indicating the same tendency as that found in vertical bubbly flows.

Verification of the measured velocities was undertaken by comparing the weighted mean velocities $\bar{u}_b$ and $\bar{u}_G$ based on the probe measurements and the measured gas volumetric flow rates $\dot{Q}_G$, respectively. $\bar{u}_b$ and $\bar{u}_G$ are defined as follows:

$$\bar{u}_b \equiv \frac{\int_A \epsilon u_b \, dA}{\int_A \epsilon \, dA} = \frac{\langle \epsilon u_b \rangle}{\langle \epsilon \rangle} = \frac{\langle j_b \rangle}{\langle \epsilon \rangle} \qquad [19]$$

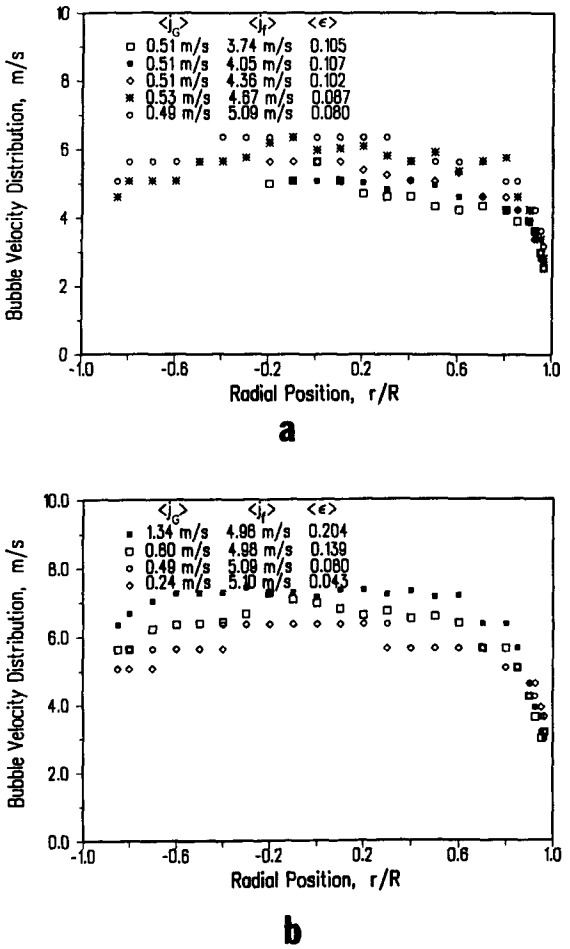

Figure 13. Bubble interface velocity distribution: (a) effect of liquid flow; (b) effect of gas flow.

and

$$\tilde{u}_G \equiv \frac{\dot{Q}_G}{\langle \epsilon \rangle A} = \frac{\langle j_G \rangle}{\langle \epsilon \rangle}, \qquad [20]$$

where the $\langle \ \ \rangle$ denote area-averaged values from integration and $\dot{Q}_G$ is the volumetric flow rate of the air.

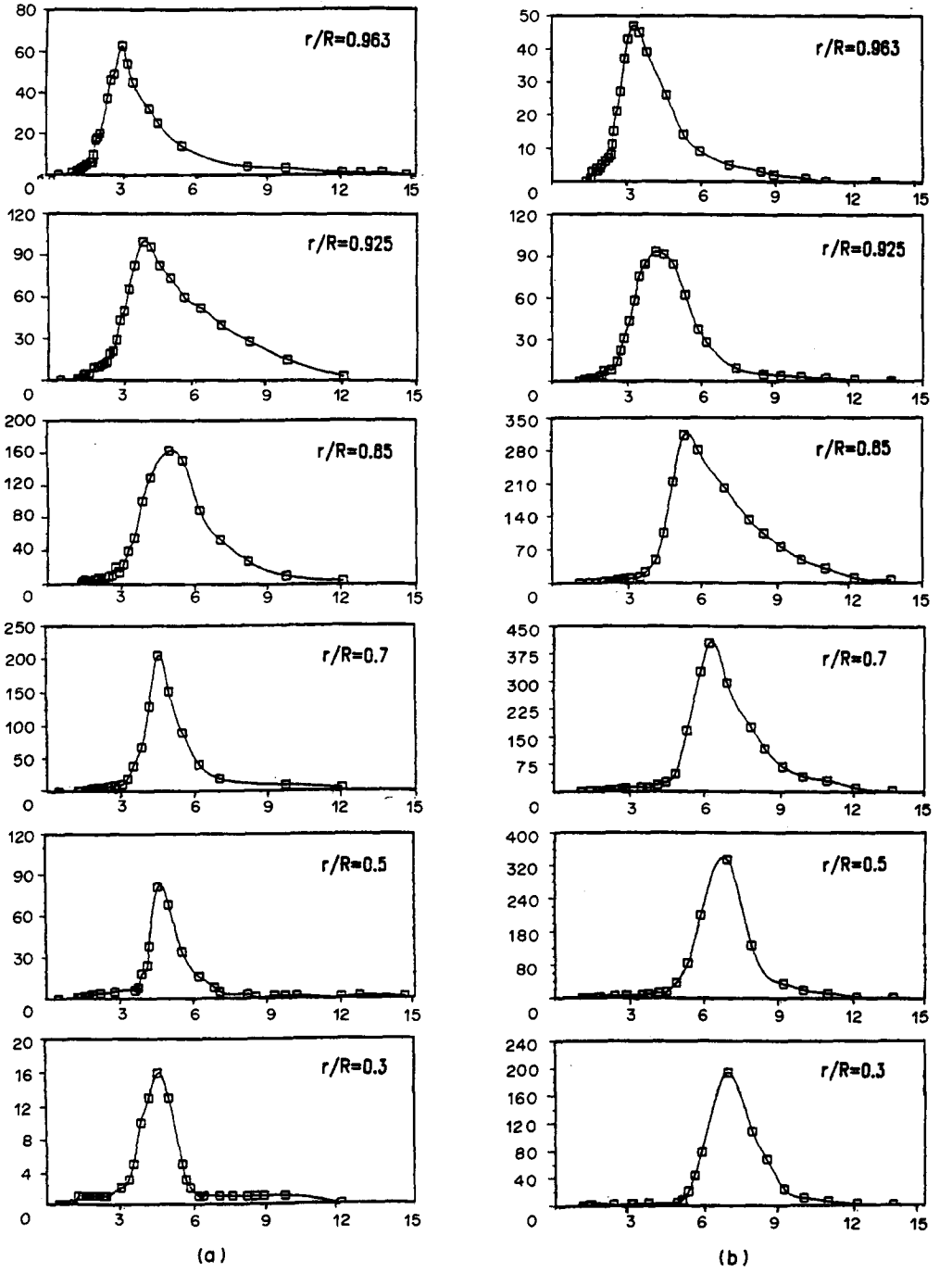

Figure 14. Typical bubble interface velocity spectra: (a) $\langle j_f \rangle = 3.83$ m/s, $\langle j_G \rangle = 0.72$ m/s, $\langle \epsilon \rangle = 0.152$; (b) $\langle j_f \rangle = 4.96$ m/s, $\langle j_G \rangle = 1.34$ m/s, $\langle \epsilon \rangle = 0.204$.

The corresponding values of the velocity from [19] were determined by numerical integration, and the values are listed in table 1. Furthermore, the deviations of $\bar{u}_b$ with respect to $\bar{u}_G$ and of $\langle j_b \rangle$ with respect to $\langle j_G \rangle$, which are, respectively, defined as

$$\Delta \bar{u}_b \equiv \frac{\bar{u}_b - \bar{u}_G}{\bar{u}_G} \times 100\% \quad [21]$$

and

$$\Delta \langle j_b \rangle \equiv \frac{\langle j_b \rangle - \langle j_G \rangle}{\langle j_G \rangle} \times 100\%, \quad [22]$$

are also listed in table 1. The mean deviation between the values obtained from integration of the local flow parameters and those obtained from flow rate measurements is $\pm$ 5.7%. The integrated values are generally lower. This may be explained partially by the fact that we expect the measured values of velocity to be slightly low, both because of the possible deflection of the bubbles when they hit the probe tips and because of missing the smallest size bubbles. In all cases, the difference is $< 12\%$ of the value calculated from the overall gas flow rate. The comparison justifies the reliability of the double-sensor resistivity probe technique for measuring local void fractions and axial velocity components.

Based on the bubble velocity and void fraction measurements, a drift-flux presentation is illustrated in figure 15. As suggested by Ishii (1977) and Wallis (1969), it is given by

$$\bar{u}_G = \bar{u}_{Gj} + c_0 \langle j \rangle \quad [23]$$

where $\bar{u}_{Gj}$ is the weighted mean drift velocity of the gas phase and c_0 is the distribution parameter. Figure 15 indicates a linear relationship between $\bar{u}_G$ and $\langle j \rangle$, which is used to determine $\bar{u}_{Gj}$ and c_0. Regression analysis on the data yields $c_0 = 1.05$ and $u_{Gj} = 0.13$ m/s. It is to be noted that such a representation was obtained from our air–water bubbly flow data which is far from the origin. Therefore, it has the limitations of our data range. It should be checked further for a wider data range.

4.4. Bubble chord-length and frequency distributions

The local bubble chordlength was determined from the bubble residency time measured from the front probe, τ, and from the bubble velocity, u_b, as follows:

$$l_{cl} = u_b \tau. \quad [24]$$

A typical bubble chord-length distribution is illustrated in figure 16(a, b). For each experiment, this type of figure has been produced to verify the order of Sauter mean diameter values obtained from [18].

The local bubble impaction rate or bubble frequency, which is the number of bubbles detected by the front probe in unit time at a specific location, can also be obtained from the experimental data. A typical bubble impaction rate distribution is shown in figure 17(a, b). It is important to

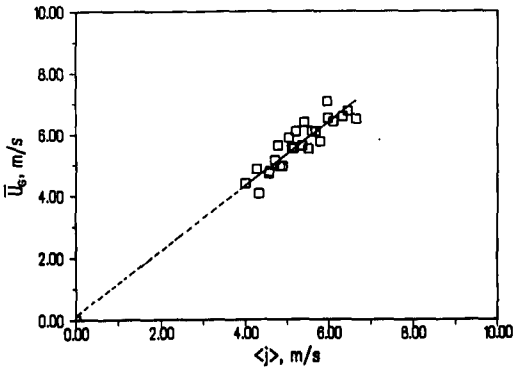

Figure 15. $\bar{u}_G - \langle j \rangle$ presentation.

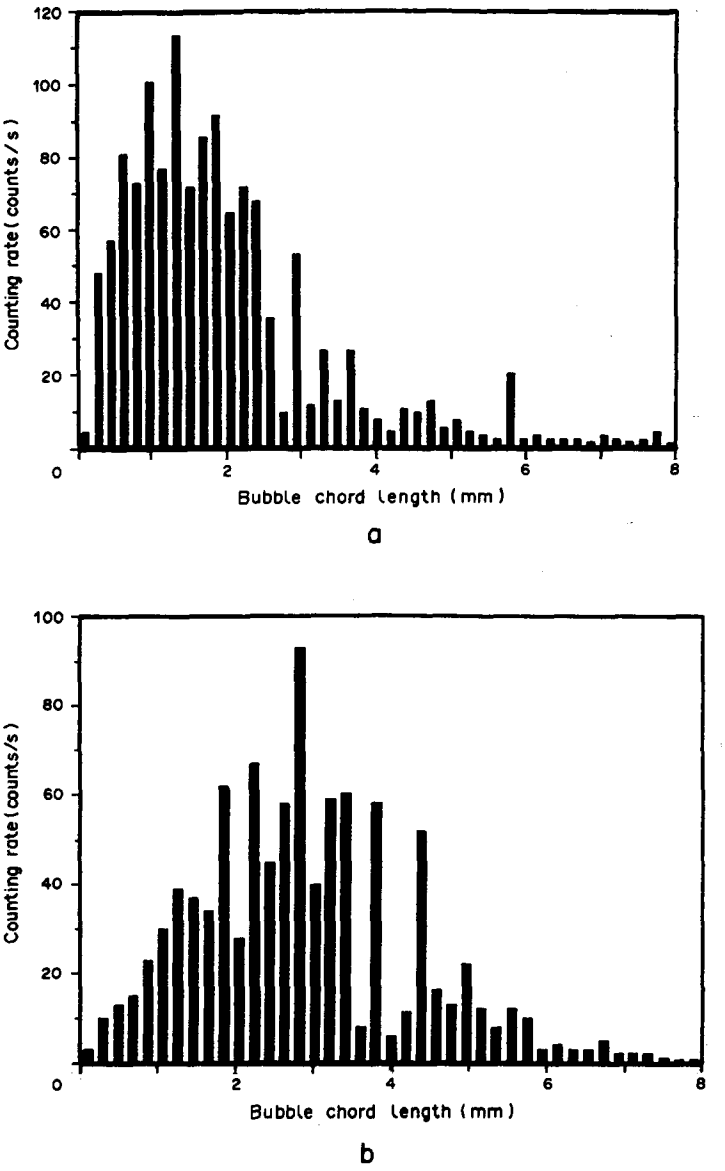

Figure 16. Typical bubble chord-length spectra ($\langle j_f \rangle = 4.96$ m/s, $\langle j_G \rangle = 1.34$ m/s, $\langle \epsilon \rangle = 0.204$) at: (a) $r/R = 0.963$; (b) $r/R = 0.3$.

note from these figures that the bubble impaction rate distribution has the same behavior as that of the local void fraction distribution. Due to the buoyancy effect, the uniformly generated and distributed bubbles move into the upper sections and crowd together near the top wall of the horizontal flow channel. A distinct peak of bubble impaction rates close to the top wall can be observed in all flow conditions, even though the bubble impaction rate profile tends to flatten as the average void fraction is increased. A very high bubble frequency on the order of 2200/s may be observed toward the top of the tube. This might explain the high void fractions and interfacial areas observed in the present horizontal bubbly flow experiments.

5. SUMMARY AND CONCLUSIONS

The internal phase distribution of cocurrent, air–water bubbly flow in a 50.3 mm dia transparent pipeline has been experimentally investigated by using a double-sensor resistivity probe technique. Liquid and gas volumetric superficial velocities ranged from 3.74 to 5.71 and 0.25 to 1.37 m/s,

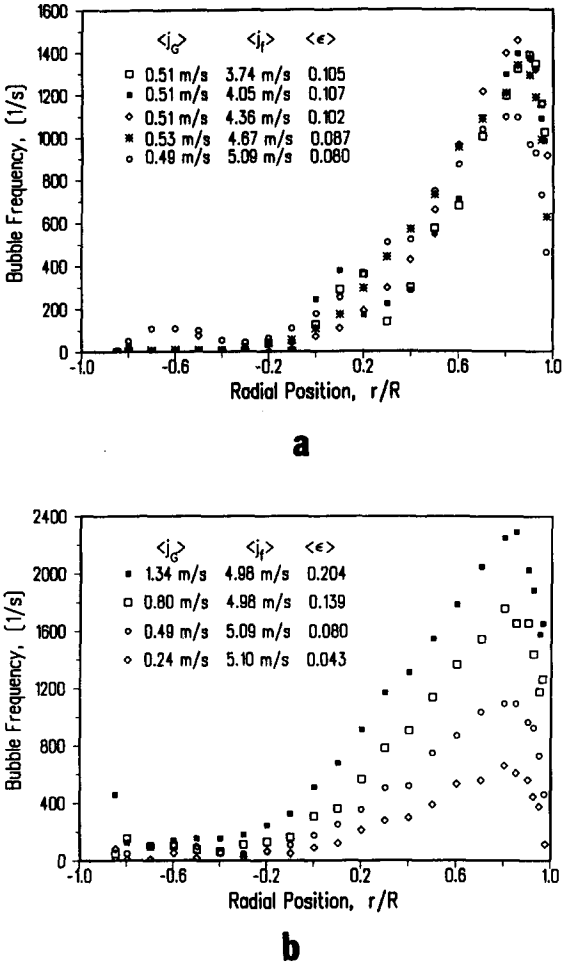

Figure 17. Bubble frequency profiles: (a) effect of liquid flow; (b) effect of gas flow.

respectively, and average void fractions ranged from 4.30 to 22.5%. The local values of void fraction, interfacial area concentration, mean bubble diameter and bubble interfacial velocity, chord-length and frequency distributions were measured.

The experimental results indicated that the void fraction, interfacial area concentration and bubble frequency have local maxima near the upper pipe wall, and that the profiles tended to flatten with increasing void fraction. For the horizontal bubbly flow, the observed peak void fraction can reach 0.65, and the peak interfacial area concentration can go up to 1000 m^2/m^3, whereas the bubble frequency may reach a value of 2200/s. It was found that either decreasing the liquid flow at constant gas flow or increasing the gas flow at a fixed liquid flow would increase the local void fraction, interfacial area concentration and the bubble frequency.

The axial bubble interface velocity showed a relatively uniform distribution except near the upper pipe wall, where a sharp reduction in velocity was found. The local bubble interface velocity and the bubble velocity turbulent fluctuations increase with the gas flow.

Using the relation between the local interfacial area concentration, void fraction and the Sauter mean diameter of bubbles, the mean bubble diameter distributions were calculated. It was observed that the mean bubble diameters ranged from 2 to 5 mm, depending on the location and flow conditions. The bubble diameter generally increases with the gas flow rate at a given liquid flow rate, although the effect was not found to be significant.

Finally, it is to be noted that the lateral phase distribution for horizontal flow and bubble size distribution are strongly affected by inlet conditions and boundaries. In the present studies, the mixing chamber that is described in section 3.1 was fixed throughout the experiments, and probe tracing was done along the vertical axis of the pipe. Therefore, it is recommended that future work

include a series of experimental studies to understand how inlet conditions and wall affect the lateral phase distribution for horizontal flow.

Acknowledgement—The work reported in this paper was supported by a grant from the U.S. Department of Energy (DE-FGO2-87ER13764).

REFERENCES

AKITA, K. & YOSHIDA, F. 1974 Bubble size, interfacial area, and liquid-phase mass transfer coefficient in bubble columns. *Ind. Engng Chem. Process Des. Dev.* **13,** 84–90.

BEATTIE, D. R. H. 1972 Two-phase flow structure and mixing length theory. *Nucl. Engng Des.* **2,** 46–64.

BENSLER, H. P., DELHAYE, J. M. & FAVREAU, C. 1987 Measurement of interfacial area in bubbly flows by means of ultrasonic technique. Presented at the *Natn. Heat Transfer Conf.*, Pittsburgh, Pa.

BOURÉ, J. A. 1978 Mathematical modelling of two-phase flows. In *Proceedings of CSNI Specialist Meeting*, Vol. 1 (Edited by BANERJEE, S. & WEAVER, K. R.), p. 85. AECL, Toronto, Ontario.

BURGESS, J. M. & CALDERBANK, P. H. 1975 The measurement of bubble parameters in two-phase dispersions—I. The development of an improved probe technique. *Chem. Engng Sci.* **30,** 743–750.

CALDERBANK, P. H. 1958 Physical rate processes in industrial fermentation, Parts I and II. *Trans. Inst. chem. Engrs* **36,** 443–463.

DANCKWERTS, P. V. 1970 *Gas–Liquid Reactions.* McGraw-Hill, New York.

HERRINGE, R. A. & DAVIS, M. R. 1976 Structural development of gas–liquid mixture flows. *J. Fluid Mech.* **73,** 97–123.

HILGERT, W. & HOFMANN, H. 1986 Characterization of gas phase flow in bubble columns of low superficial gas velocities with the aid of ultrasonic doppler techniques. *Gen. Chem. Engng* **9,** 180–190.

HOFFER, M. S. & RESNICK, W. 1975 A modified electroresistivity probe technique for steady- and unsteady-state measurements in fine dispersions—I. Hardware and practial operating aspects. *Chem. Engng Sci.* **30,** 473–480.

ISHII, M. & KOCAMUSTAFAOGULLARI, G. 1982 Two-phase flow models and their limitations. Presented at the *NATO Advanced Research Wkshp on Advances in two-phase Flow and Heat Transfer*, Spitzingsee, Fed. Rep. Germany.

ISHII, M. & MISHIMA, K. 1981 Study of two-fluid model and interfacial area. Argonne National Lab. Report ANL-80-111.

JONES, S. W., AMBLAND, A. & FAVREAU, C. 1986 Interaction of an ultrasonic wave with a bubbly mixture. *Expts Fluids* **4,** 341–349.

KATAOKA, I., ISHII, M. & SERIZAWA, A. 1985 Interfacial area in two-phase flow; formulation and measurement. Presented at the *23rd Natn. Heat Transfer Conf. ASME*, Denver, Colo.

LIU, T. T.-J. 1989 Experimental investigation of turbulence structure in two-phase bubbly flow. Ph.D. Thesis, Northwestern Univ., Evanston, Ill.

MATSUI, G. 1984 Characteristic structure of upward bubble flow under the same flow rate conditions. Presented at the *Japan–U.S. Semin. on Two-phase Flow Dynamics*, Lake Placid, N.Y.

MCLAUGHLIN, C. M. & RUSHTON, J. H. 1973 Interfacial areas of liquid–liquid dispersions from light transmission measurements. *AIChE Jl* **19,** 813–822.

MICHIYOSHI, I. & SERIZAWA, A. 1986 Turbulence in two-phase bubbly flow. *Nucl. Engng Des.* **95,** 253–267.

NEAL, L. G. & BANKOFF, S. G. 1963 A high resolution resistivity probe for determination of local void properties in gas–liquid flow. *AIChE Jl* **9,** 490–494.

OHBA, K. & ITOH, T. 1978a Light attenuation technique for void fraction measurement in two-phase bubbly flow—I. Theory. *Technol. Rep. Osaka Univ.* **28**(1448), 487–494.

OHBA, K. & ITOH, T. 1978b Light attenuation technique for void fraction measurement in two-phase bubbly flow—II. Experiment. *Technol. Rep. Osaka Univ.* **28**(1449), 495–506.

OHBA, K., ITOH, T. & YUHARA, T. 1978 Light attenuation technique for void fraction measurement in two-phase bubbly flow—III. Effect of some parameters on accuracy of measurement. *Technol. Rep. Osaka Univ.* **28**(1450), 507–516.

PARK, W. H., KANG, W. K., CAPES, C. E. & OSBERG, G. L. 1969 The properties of bubbles in fluidized beds of conducting particles as measured by an electroresistivity probe. *Chem. Engng Sci.* **24,** 851–865.

RIGBY, G. R., VAN BLOCKLAND, G. P., PARK, W. H. & CAPES, C. E. 1970 Properties of bubbles in three phase fluidized beds as measured by an electroresistivity probe. *Chem. Engng Sci.* **25,** 1729–1741.

SCHUMPE, A. & DECKWER, W. D. 1980 Analysis of chemical methods of determination of interfacial area in gas-in-liquid dispersions with non-uniform bubble size. *Chem. Engng Sci.* **35,** 2221–2233.

SCHUMPE, A. & DECKWER, W. D. 1982 Comparison of the photographic and the sulfite oxidation method for interfacial area determination in bubble columns. *Chem. Engng Commun.* **17,** 313–324.

SERIZAWA, A., KATAOKA, I. & MICHIYOSHI, I. 1975 Turbulence structure of air-water bubbly flow—I. Measuring techniques. *Int. J. Multiphase Flow* **2,** 221–233.

SHARMA, M. M. & DANCKWERTS, P. V. 1970 Chemical methods for measuring interfacial area and mass transfer coefficients in two-fluid systems. *Br. chem. Engng* **15,** 522–528.

STRAUS, A. A., VON STOCKER, U. & REILLY, P. J. 1986 Measurement of interfacial areas in aerobic fermentations by ultrasonic pulse transmission. *Biotechnol. Bioengng* **28,** 1302–1309.

VAN DER WELLE, R. 1985 Void fraction, bubble velocity and bubble size in two-phase flow. *Int. J. Multiphase Flow* **11,** 317–345.

VETEAU, J. M. 1981 Contribution a l'etude des techniques de measure de l'aire interfacial dans les écoulements a bulles. Sc.D. Thesis, National Grenoble Polytechnic Inst., France.

VETEAU, J. M. & CHARLOT, R. 1981 Techniques de measure des aires intefacials dans les écoulements a bulles—III. Comparison de la méthode d'attenuation d'un faisceau. Lumineux et d'une Méthode Locale. CEA Report CEA-R-5122, France.

VETEAU, J. M. & MOREL, Y. 1982 Techniques de measures des aires interfacials dans les écoulements a bulles—II. La méthode chimique. CEA Report CEA-R-5092, France.

WALLIS, G. B. 1969 *One-dimensional Two-phase Flow*, pp. 261–263. McGraw-Hill, New York.

WANG, S. K. 1985 Three-dimensional turbulence structure measurements in air/water two-phase flow. Ph.D. Thesis, Rensselaer Polytechnic Inst., Troy, NY.

WANG, S. K., LEE, S. J., JONES, O. C. JR and LAHEY, R. T. JR 1987 Three-dimensional turbulence structure and phase distribution measurements in bubbly two-phase flow. *Int. J. Multiphase Flow* **13,** 327–340.

YANZ, N. S., SHEN, Z. Q., CHEN, B. H. & MCMILLAN, A. F. 1986 Pressure drop, gas holdup, and interfacial area for gas–liquid contact in karr columns. *Ind. Engng Chem. Process Des. Dev.* **25,** 660–664.